NUCLEAR THEORY, Vol. 41 (2024)
eds. M. Gaidarov, N. Minkov, Heron Press, Sofia

Rearrangement Terms in Relativistic Point Coupling Models in Second Tamm-Dancoff Approximation

D. Vale[1], **N. Paar**[2]

[1]Istrian University of Applied Sciences, Riva 6, 52100 Pula, Croatia
[2]Department of Physics, Faculty of Science, University of Zagreb, Bijenička cesta 32, 10000 Zagreb, Croatia

Abstract. Theoretical description of collective excitations in nuclei and astrophysically relevant processes involving nuclear excited states requires approaches going beyond Random Phase Approximation (RPA), based on 1 particle and 1 hole ($1p1h$) configurations in order to assess the fine structure of the excitation spectra. To realistically compare theoretical predictions with experimental data, it is essential to microscopically describe the fragmentation of excited state spectrum by introducing couplings with complex configurations. We have developed self-consistent Second Tamm-Dancoff Approximation (STDA) based on the relativistic energy density functional theory. This approach allows for a more accurate and comprehensive analysis of nuclear excitations by incorporating the complex interplay of $1p1h$ and $2p2h$ configurations. This work is focused on analyzing isoscalar monopole and quadrupole transitions in ^{40}Ca and ^{48}Ca within the framework of STDA. We have used DD-PC1 parametrization of the relativistic point coupling interaction and investigated the influence of rearrangement terms on the excitation spectra, the position of centroid energies, and the strength distribution.

1 Introduction

Nuclear structure research is fundamental for understanding various phenomena in both nuclear physics and astrophysics. One of the significant challenges in this field is the accurate description of collective multipole excitations, such as giant resonances. These excitations play a crucial role in interpreting experimental data and advancing theoretical models.

In this work, we present the first self-consistent implementation of the Second Tamm-Dancoff Approximation (STDA) based on the relativistic energy density functional theory. We have analyzed both isoscalar giant monopole (ISGMR) and quadrupole excitations (ISGQR) in ^{40}Ca and ^{48}Ca. Despite being computationally more intensive, STDA delivers greater accuracy and the insight into fragmentation in modeling complex excitation spectra. Both STDA and second random phase approximation (SRPA) were introduced in [1] and applied in a few nuclear models which included finite range interactions [2, 3], Skyrme

functionals [4, 5] and Gogny interaction [6]. While previous STDA and SRPA studies have been primarily focused on nonrelativistic models, often with limited configurations, our approach incorporates the full complexity of these nuclear transitions in the relativistic energy density functional (REDF) theory with an exception of neglecting coupling between 2 particle-2 hole ($2p2h$) configurations in the present implementation, thus providing a comprehensive understanding of the excitation spectra in the relativistic framework.

.

2 Relativistic Lagrangian

Two types of effective nuclear interactions are most commonly present in modern REDF theory: (i) the Walecka-type (nucleons represent a system of Dirac particles interacting through meson and photon exchange); (ii) the contact type (point-coupling, where the meson propagator is replaced by a zero-range interaction) [7]. In both models, the relativistic Lagrangian is constructed using the fundamental symmetries of QCD (Lorentz covariance, gauge invariance, and chiral symmetry). The relativistic point-coupling Lagrangian is built from basic densities and currents that are bilinear in the Dirac spinor fields for nucleons [7–9]:

$$\bar{\psi} O_\tau \Gamma \psi, \;\; O_\tau \in \{1, \tau_i\}, \quad \Gamma \in \{1, \gamma_\mu, \gamma_5, \gamma_s \gamma_\mu, \sigma_{\mu v}\}. \tag{1}$$

where τ_i are the Pauli matrices in isospin space, and Γ represents the Dirac matrices or their products. The determination of the ground state density and energy arises from the self-consistent solution of the relativistic linear single-nucleon Kohn-Sham equations. The general expression for the effective Lagrangian can be written using an expansion of currents $\bar{\psi}\, O\, \tau\, \Gamma\, \psi$ and their derivatives. Following the analogy of the Walecka type models, i.e., the expansion of propagators, one can easily construct four-fermion (contact) interaction in terms of different isospin-spatial space ph channels: i) isoscalar-scalar $(\bar{\psi}\psi)(\bar{\psi}\psi)$, ii) isoscalar-vector $(\bar{\psi}\gamma_\mu\psi)(\bar{\psi}\gamma^\mu\psi)$, iii) isovector-scalar $(\bar{\psi}\vec{\tau}\psi)(\bar{\psi}\vec{\tau}\psi)$ and iv) isovector-vector $(\bar{\psi}\vec{\tau}\gamma_\mu\psi)(\bar{\psi}\vec{\tau}\gamma^\mu\psi)$. In a similar manner, the derivative terms can also be constructed. Upon including the free-nucleon and electromagnetic components, the resulting Lagrangian density for the nuclear system is given by the expression [7]:

$$\begin{aligned}\mathcal{L} \;&= \bar{\psi}\left(i\gamma_\mu\partial^\mu - m\right)\psi - \frac{1}{2}\alpha_S(\rho)\left(\bar{\psi}\psi\right)\left(\bar{\psi}\psi\right) \\ &- \frac{1}{2}\alpha_V(\rho)\left(\bar{\psi}\gamma_\mu\psi\right)\left(\bar{\psi}\gamma^\mu\psi\right) - \frac{1}{2}\alpha_{TV}(\rho)\left(\bar{\psi}\vec{\tau}\gamma_\mu\psi\right)\left(\bar{\psi}\vec{\tau}\gamma^\mu\psi\right) \\ &- \frac{1}{2}\delta_S\partial_\nu\left(\bar{\psi}\psi\right)\partial^\nu\left(\bar{\psi}\psi\right) - e\bar{\psi}\gamma_\mu A^\mu\frac{1-\tau_3}{2}\psi. \end{aligned} \tag{2}$$

Density dependence in the case of the isoscalar-scalar $\alpha_S(\rho)$, isoscalar-vector $\alpha_V(\rho)$ and isovector-vector coupling $\alpha_{TV}(\rho)$ for the DD-PC1 parametrization

of the point coupling Lagrangian density from eq. (2) is given by

$$\alpha_i\left[x\right] \;=\; a_i + (b_i + c_i x)\exp(-d_i x), \tag{3}$$

where $x = \rho/\rho_{sat}$, ρ stands for barion (vector) density and ρ_{sat} for the nucleon density at saturation in the symmetric nuclear matter. The values of parameters $a_i,\ b_i,\ c_i$ and d_i for the DD-PC1 parametrization used in this work are given in Ref. [7].

3 Second TDA

In the relativistic form of TDA the excitation operators are assumed to be linear superposition of $1p1h$ and antiparticle-hole ($1a1h$) operators:

$$Q^\dagger_\nu \;=\; \sum_{ph} X^\nu_{ph} a^\dagger_p a_h + \sum_{\alpha h} X^\nu_{\alpha h} a^\dagger_\alpha a_h. \tag{4}$$

For the simplicity, the coupling to total angular momentum is not included here. In the case of the relativistic STDA, we need to include $2p2h$, 1 particle1 antiparticle2 hole ($1p1a2h$) and 2 antiparticle2 hole ($2a2h$) pairs, in addition to the standard ones from eq. (4):

$$\begin{aligned} Q^\dagger_\nu \;=\; &\sum_{ph} X^\nu_{ph} a^\dagger_p a_h + \sum_{\alpha h} X^\nu_{\alpha h} a^\dagger_\alpha a_h + \sum_{p<p'h<h'} \mathcal{X}^\nu_{pp'hh'} a^\dagger_p a^\dagger_{p'} a_{h'} a_h \\ &+ \sum_{p\alpha h<h'} \mathcal{X}^\nu_{p\alpha hh'} a^\dagger_p a^\dagger_\alpha a_{h'} a_h + \sum_{\alpha<\alpha'h<h'} \mathcal{X}^\nu_{\alpha\alpha'hh'} a^\dagger_\alpha a^\dagger_{\alpha'} a_{h'} a_h. \end{aligned} \tag{5}$$

The energies E_ν of the excited states and their X and $\mathcal{X}$ amplitudes are obtained by solving STDA eigenvalue problem:

$$\begin{pmatrix} A_{11} & A_{12} \\ A_{21} & A_{22} \end{pmatrix} \begin{pmatrix} X^\nu \\ \mathcal{X}^\nu \end{pmatrix} = E_\nu \begin{pmatrix} X^\nu \\ \mathcal{X}^\nu \end{pmatrix}. \tag{6}$$

with amplitudes $X^\nu = (X^\nu_{ph}\ X^\nu_{\alpha h})^T$ and $\mathcal{X}^\nu = (\mathcal{X}^\nu_{pp'hh'}\ \mathcal{X}^\nu_{p\alpha hh'}\ \mathcal{X}_{\alpha\alpha'hh'})^T$. In the present work we neglect $1p1\alpha2h$ and $2\alpha2h$ contributions in $Q^\dagger_\nu$ (and $\mathcal{X}^\nu$), therefore we solve the STDA equations in $ph \oplus ah \oplus 2p2h$-space. Furthermore, if we disregard the coupling among $2p2h$ states, the matrix A_{22} becomes diagonal, with its elements corresponding to the unperturbed $2p2h$ energies:

$$A_{22} = \delta_{p_1p'_1}\delta_{h_1h'_1}\delta_{p_2p'_2}\delta_{h_2h'_2}\left(e_{p_1} + e_{p_2} - e_{h_1} - e_{h_2}\right). \tag{7}$$

Standard TDA, i.e., A_{11} matrix elements in the STDA, within density functional (DFT) framework are given by (see Ref. [10] or [11]):

$$\begin{aligned}[A_{11}]_{Ph;P'h'} = \frac{1}{2}\sum_{ij}\left[\frac{\partial^2\hat{v}_{ijij}\left[\rho\right]}{\partial\rho_{hP}\partial\rho_{P'h'}}\right]\Bigg|_{\rho\,=\,\rho^{(0)}} + \sum_{j}\left[\frac{\partial\hat{v}_{Pjhj}\left[\rho\right]}{\partial\rho_{P'h'}}\right]\Bigg|_{\rho=\rho^{(0)}} \\ + \sum_{j}\left[\frac{\partial\hat{v}_{h'jP'j}\left[\rho\right]}{\partial\rho_{hP}}\right]\Bigg|_{\rho=\rho^{(0)}} + \lambda_{PP'}\left[\rho^{(0)}\right]\delta_{hh'} \\ - \lambda_{h'h}\left[\rho^{(0)}\right]\delta_{PP'} + \hat{v}_{Ph'hP'}\left[\rho^{(0)}\right]. \end{aligned} \tag{8}$$

The first three terms in eq. (8) are the so called rearrangement terms, which exist in ph channels with density dependent couplings (see eq. (2)). In the relativistic case, indices P and P' in eq. (8) are used for both particle and antiparticle states, while p, p_i and p_i' stand for particle, and h, h_i and h_i' for hole states ($i = 1$ or 2). The present notation for the two-body interaction $\hat{v}_{abcd}$ obeys standard Feynman rules. The coupling between 1p1h and 2p2h configurations is incorporated into the matrix A_{12} element, which is given by the following expression [1]:

$$\begin{aligned}A^{12}_{[ph];[p_1p_2h_1h_2]} = \mathcal{A}(p_1,p_2)\mathcal{A}(h_1,h_2)\delta_{pp_1}\delta_{hh_1}\lambda_{h_2p_2}\left[\rho^{(0)}\right] \\ + \mathcal{A}(h_1,h_2)\delta_{hh_1}\hat{v}_{ph_2p_1p_2}\left[\rho^{(0)}\right] - \mathcal{A}(p_1,p_2)\delta_{pp_1}\hat{v}_{h_1h_2hp_2}\left[\rho^{(0)}\right], \end{aligned} \tag{9}$$

with antisymmetrization $\mathcal{A}(a,b) = 1 - P(a,b)$, where $P(a,b)$ is permutation operator which acts on all quantum numbers in a and b. For the A_{12} rearrangement term we have the following term (for the derivation see Ref. [10]):

$$\left[A^{\text{rear. term}}_{12}\right]_{ph;p_1p_2h_1h_2} = \left.\frac{\partial\hat{v}_{h_1h_2p_1p_2}\left[\rho\right]}{\partial\rho_{hp}}\right|_{\rho=\rho^{(0)}}, \tag{10}$$

in the isoscalar-scalar, isoscalar-vector and isovector-vector ph channel.

4 Results

In Figures 1 and 2, we show discrete ISGMR strength distribution for the ph free response, TDA and STDA response in ^{40}Ca and ^{48}Ca. To obtain the nuclear ground state in the Dirac-Hartree model with the relativistic point coupling interaction DD-PC1 [7], the single-particle energies and wave functions of the occupied and unoccupied levels are solved by using the spherical harmonic oscillator basis expanded up to the maximum major quantum number of $N_{max} = 20$ for protons and neutrons both for ^{40}Ca and ^{48}Ca. Both TDA and STDA calculations used ph cutoff $E_{ph} = 100$ MeV and ah cutoff of $E_{ah} = 1800$ MeV. We observed the fragmentation of the spectrum for both nuclei even with relatively small 2p2h $E_{\text{cutoff}} \approx 40$ MeV. In the STDA framework, as the energy cutoff parameter E_{cutoff} for 2p2h configurations is increased, a rapidly growing number of

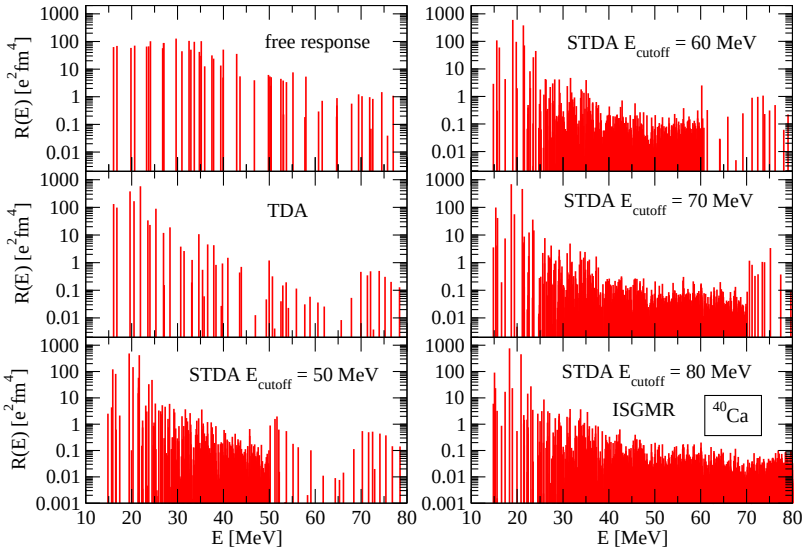

Figure 1. Isocalar giant monopole resonance strength distribution (ISMGR) in ^{40}Ca for ph free response, TDA and STDA responses as functions of excitation energy for different 2p2h energy cutoffs.

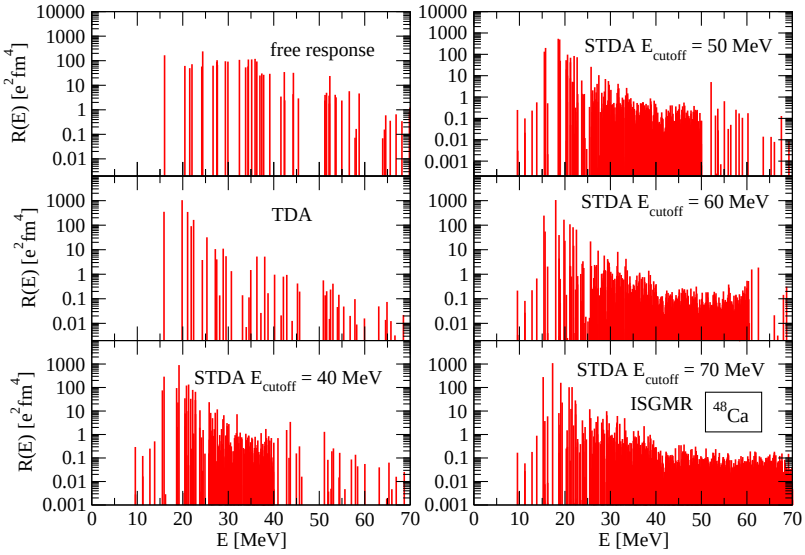

Figure 2. The same as Figure 1, but for ^{48}Ca.

states emerge between the primary $1p1h$ peaks. For instance, in the case of ^{40}Ca, the number of such states increases from a few hundred at $E_{\text{cutoff}} = 30$ MeV to nearly 20,000 when E_{cutoff} reaches 80 MeV. While the majority of these additional states are predominantly of $2p2h$ character, few of them exhibit a strong mixing of $1p1h$ and $2p2h$ configurations.

In Figures 3 and 4, the calculated distributions for ph free response, TDA and STDA have been convoluted with a Lorentzian function with a 1 MeV width, which introduces an artificial width to all peaks. The STDA centroid energies are slightly different than those obtained from TDA. In particular, for the ISGMR in ^{40}Ca we obtained $E^{\text{STDA}}_{\text{centroid}} = 21.194$ MeV ($E^{\text{TDA}}_{\text{centroid}} = 21.192$ MeV) and full width $\Gamma^{\text{STDA}} = 6.377$ MeV for 2p2h $E_{\text{cutoff}} = 60$ MeV, while experimental values are somewhat lower with $E^{\text{exp.}}_{\text{centroid}} = (19.18 \pm 0.37)$ MeV and rms width of $\Gamma^{\text{exp.}} = 4.88$ MeV [12]. On the other hand, for the ISGMR in ^{48}Ca we obtained $E^{\text{STDA}}_{\text{centroid}} = 20.122$ MeV ($E^{\text{TDA}}_{\text{centroid}} = 20.125$ MeV) and full width $\Gamma^{\text{STDA}} = 6.818$ MeV for 2p2h $E_{\text{cutoff}} = 60$ MeV. The experimental value of centroid energy is somewhat lower for ISGMR in ^{48}Ca with $E^{\text{exp.}}_{\text{centroid}} = (19.5 \pm 0.1)$ MeV (for TAMU group $E^{\text{exp.}}_{\text{centroid}} = (19.9 \pm 0.2)$ MeV) [13]. Although the centroid energies differ only slightly between TDA and STDA, a shift of the dominant peaks in STDA towards lower energies is observed for both nuclei, reaching up to $|\Delta E_x| \approx 2$ MeV for $E_{\text{cutoff}} = 60$ MeV relative to TDA. The primary reason for the discrepancy between the TDA and STDA results for the ISGMR lies in the fact that the collective excitations examined here are influenced by the implicit inclusion of the coupling between single-particle states and virtual phonons within STDA, although only partially, due to the exclusion of direct

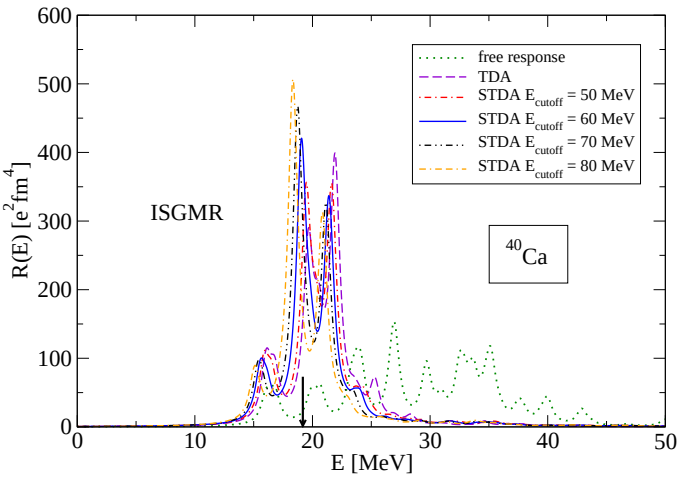

Figure 3. ISGMR strength distribution in ^{40}Ca for ph free response, TDA and STDA responses as functions of excitation energies for different 2p2h energy cutoffs. Lorentzian smoothing of 1 MeV width is used. The experimental value of centroid energy is represented by an arrow.

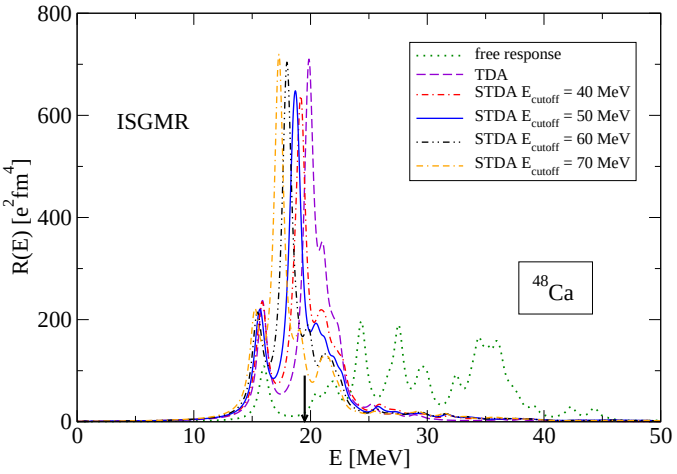

Figure 4. The same as Figure 3, but for ^{48}Ca.

coupling between $2p2h$ states. The inclusion of higher-order configurations in STDA modifies the single-particle states with self-energy corrections, narrowing their energy spacing and thus decreasing the ph excitation energies [3]. The rearrangement terms in A_{12} matrix are included in all STDA calculations, however, they do not significantly affect the excitation spectrum.

Figures 5 and 6 show the discrete ISGQR strength distributions corresponding to the free response, TDA and STDA responses for ^{40}Ca and ^{48}Ca, respectively. For the ISGQR in ^{40}Ca we obtained $E^{\text{STDA}}_{\text{centroid}} = 18.138$ MeV ($E^{\text{TDA}}_{\text{centroid}} = 19.369$ MeV) and full width $\Gamma^{STDA} = 6.664$ MeV ($\Gamma^{TDA} = 2.109$ MeV) for $E_{\text{cutoff}} = 60$ MeV, while experimental values are $E^{\text{exp.}}_{\text{centroid}} = (17.84 \pm 0.43)$ MeV and rms width $\Gamma^{\text{exp.}} = (2.89 \pm 0.60)$ MeV [12]. In the case of the STDA calculation of ISGQR in ^{48}Ca the centroid energy $E^{\text{STDA}}_{\text{centroid}} = 16.418$ MeV and the full width $\Gamma^{\text{exp.}} = 7.558$ MeV. The difference between the TDA and STDA centroid energies for the ISGQR in ^{48}Ca is only $|\Delta E| \approx 0.001$ MeV. Figures 7 and 8 show smoothened strength distribution for ISGQR in ^{40}Ca and ^{48}Ca. In the case of the STDA with 2p2h $E_{\text{cutoff}} \gtrsim 60$ MeV eigenstates in the low-lying part of the ISGQR spectrum for ^{40}Ca ($E \lesssim 10$ MeV) start to appear (see Figure 5). In contrast, these states are completely absent in the TDA calculations, which do not predict any strength in this region. For example, when E_{cutoff} is set to 60 MeV, three states are generated at excitation energies of 5.245, 8.775, and 10.083 MeV, with corresponding transition strengths of 7.620, 58.067, and 1.396 e^2 fm^4, respectively. On the other hand, the obtained low-lying TDA spectrum in ^{48}Ca contains one dominant peak at $E = 3.751$ MeV with corresponding strength of $R = 91.132$ e^2 fm^4, and the smaller one with $E = 7.450$ MeV and $R = 7.483$ e^2 fm^4. For $E_{\text{cutoff}} = 55$ MeV in STDA calculation of ISGQR in ^{48}Ca, a significant portion of the transition strength below 10 MeV is concentrated mainly in

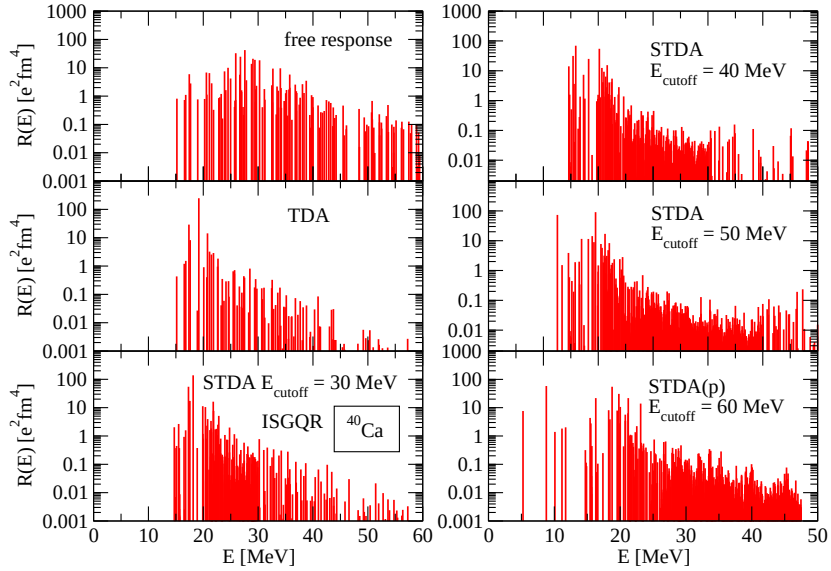

Figure 5. Discrete ISGQR strength distribution in ^{40}Ca for ph free response, TDA and STDA responses as functions of excitation energy for different 2p2h energy cutoffs. STDA(p) stands for spectrum calculated with partial eigenvalues methods.

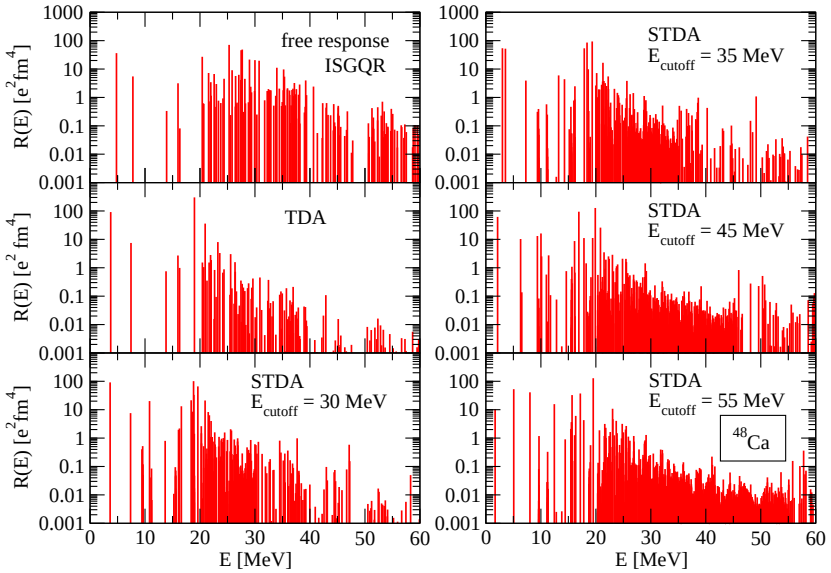

Figure 6. The same as Figure 5 but for ^{48}Ca.

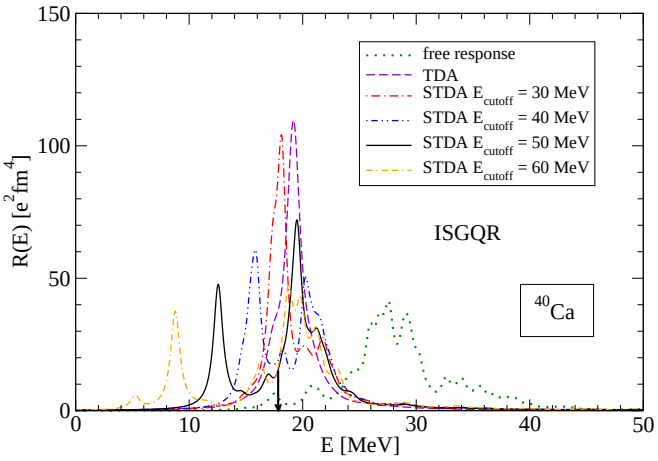

Figure 7. The ISGQR strength distribution in ^{40}Ca for the ph free response, TDA and STDA responses. For details see the description bellow Fig. 3.

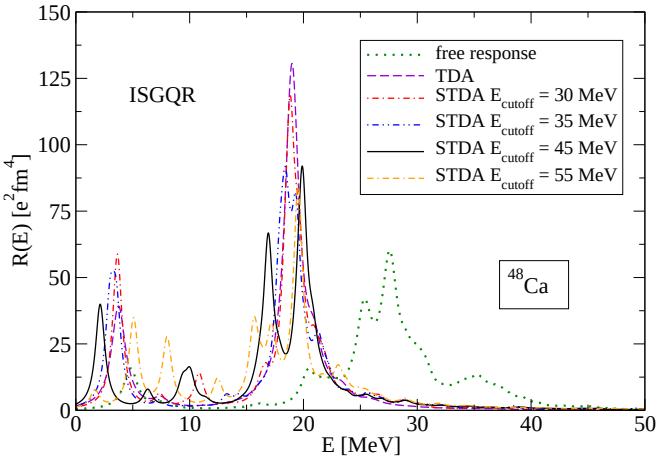

Figure 8. The same as Figure 7, but for ^{48}Ca.

three peaks, appearing at 1.675 MeV, 5.073 MeV, and 8.017 MeV. However, the total strength in this energy region amounts only 104.15 e^{2}fm^4. Experimentally, the ISGQR strength in this low-energy region is approximately 332 e^2 fm^4 for ^{40}Ca and 407 e^2 fm^4 for ^{48}Ca [14]. This discrepancy indicates that the STDA model in its diagonal approximation underestimates the experimental strength in the low-lying part of energy spectrum by about 80% in ^{40}Ca and 74% in ^{48}Ca, suggesting that certain collective or configuration-mixing effects are missing in this theoretical framework.

5 Summary and Future Perspective

In this work, we have presented the first relativistic STDA calculations based on the relativistic nuclear energy density functional with point coupling interactions. By including higher-order 2 particle-2 holes ($2p2h$) configurations, the STDA in its diagonal approximation provides a fragmentation in the representation of the ISGMR and ISGQR transition strengths, and energy shifts of the main peaks to lower energies. The STDA is capable to describe fine details in the ISGQR excitation spectra of ^{40}Ca and ^{48}Ca, including low-frequency modes that TDA may overlook. For more complete description, future studies will extend this model to second RPA, incorporating the coupling between $2p2h$ configurations, and thorough investigation of the contributions of antiparticles in $pa2h$ and $2a2h$ configurations, as well as implementation of the subtraction method.

Acknowledgments

This work is supported by the Croatian Science Foundation under the project number IP-2022-10-7773.

References

[1] J. Da Providência, *Nucl. Phys.* **61** (1965) 87-96.

[2] P. Papakonstantinou, R. Roth, *Phys. Rev. C* **81** (2010) 024317.

[3] P. Papakonstantinou, R. Roth, *26th International Workshop on Nuclear Theory*, arXiv:0709.3167 [nucl-th] (2007).

[4] D. Gambacurta, M. Grasso, F. Catara, *Phys. Rev. C* **81** (2010) 054312.

[5] F. Minato, *Phys. Rev. C* **93** (2016) 044319.

[6] D. Gambacurta, M. Grasso, V. De Donno, G. Co', F. Catara, *Phys. Rev. C* **86** (2012) 021304.

[7] T. Nikšić, N. Paar, D. Vretenar, P. Ring, *Comp. Phys. Comm.* **185** 1808.

[8] J. Daoutidis, P. Ring, *Phys. Rev. C* **80** (2009) 024309.

[9] T. Bürvenich, D. G. Madland, J.A. Maruhn, P.-G. Reinhard, *Phys. Rev. C* **65** (2002) 044308.

[10] D. Gambacurta, M. Grasso, F. Catara *J. Phys. G: Nucl. Part. Phys.* **38** (2011) 035103.

[11] P. Ring, P. Schuck, *The Nuclear Many-Body Problem*, Springer-Verlag, Berlin (1980).

[12] D.H. Youngblood, Y.-W. Lui, H.L. Clark, *Phys. Rev. C* **63** (2001) 067301. [Erratum: *Phys. Rev. C* **64** (2001) 049901].

[13] K.B. Howard, U. Garg, M. Itoh, H. Akimune, S. Bagchi, T. Doi, Y. Fujikawa, M. Fujiwara, T. Furuno, M.N. Harakeh, Y. Hijikata, K. Inaba, S. Ishida, N. Kalantar-Nayestanaki, T. Kawabata, S. Kawashima, K. Kitamura, N. Kobayashi, Y. Matsuda, A. Nakagawa, S. Nakamura, K. Nosaka, S. Okamoto, S. Ota, S. Weyhmiller, Z. Yang, *Phys. Lett. B* **801** (2020) 135185.

[14] T. Hartmann, J. Enders, P. Mohr, K. Vogt, S. Volz, A. Zilges, *Phys. Rev. C* **65** (2002) 034301.